



Ultra-High Resolution Optical Aberrometry in Patients with Keratoconus: A Cross-Sectional Study

Gonzalo Velarde-Rodriguez · Carolina Belda-Para · Miriam Velasco-Ocaña ·
Juan M. Trujillo-Sevilla · Javier Rodríguez-Martin · Ignacio Jiménez-Alfaro ·
José M. Rodríguez-Ramos · Nicolas Alejandre-Alba

Received: December 23, 2022 / Accepted: February 7, 2023 / Published online: March 1, 2023
© The Author(s) 2023

ABSTRACT

Introduction: This study performs optical aberration assessment in patients using a novel ultra-high-resolution device. The objective of this study is to analyze optical aberrations, especially the very high order wavefront (more than 10th order of Zernike coefficients), and compare between keratoconus and healthy patients.

Methods: In this cross-sectional study, we analyzed 43 eyes from 25 healthy patients and 43 eyes from 27 patients with keratoconus using corneal tomography and a very high-resolution (8.55 μm) aberrometer prototype (T-eyede) outfitted with a sensor originally developed for use

in the field of astrophysics. Corneal aberration values were assessed using an optical model built with Zemax optical software, while ocular aberrations were assessed using T-eyede. In addition, image-processing analysis was performed of the wavefront phase, creating a high-pass filter map.

Results: We found lower values for ocular aberrations than corneal aberrations in both groups ($p < 0.001$). Specifically, we found a reduction in primary astigmatism (0.145 μm) and primary coma (0.017 μm). Also, the keratoconus group showed significantly higher wavefront aberration values compared with controls ($p < 0.001$). An analysis of the high-pass filter map revealed 2 contrasting results: one smooth or clear, while the other presented a banding pattern. Almost all in the control group (95%) showed the first pattern, while 77% of the keratoconus group showed a banding pattern on the filtered map (chi-squared test, $p < 0.001$).

Conclusion: This device provides reliable, precise measurements of ocular aberrations that correlate well with corneal aberrations. Furthermore, the extraordinary high-resolution measurements revealed unprecedented micro changes in the wavefront phase of patients with keratoconus that varied with disease stage. These findings could lead to new screening or follow-up methods.

Supplementary Information The online version contains supplementary material available at <https://doi.org/10.1007/s40123-023-00684-2>.

G. Velarde-Rodriguez (✉) · I. Jiménez-Alfaro ·
N. Alejandre-Alba
Fundación Jiménez Díaz University Hospital, Avda.
Reyes Católicos, 2, Madrid, Spain
e-mail: gonzalo.velarde@quironsalud.es

C. Belda-Para · M. Velasco-Ocaña ·
J. M. Trujillo-Sevilla · J. M. Rodríguez-Ramos
Wooptix S.L. Avda, Trinidad 61 Planta 7, La Laguna,
Tenerife, Canary Islands, Spain

J. Rodríguez-Martin
Clinica Nivaria, Avda. Reyes Católicos, 25, Tenerife,
Canary Islands, Spain

Keywords: Keratoconus; Optical aberration; Optics; Aberrometry; Cornea

Key Summary Points

Why carry out this study?

This study uses a new prototype of an aberrometer with unprecedented resolution power in the ophthalmology field. This feature permitted an exhaustive analysis of the very high-order aberrations and characterize the keratoconus eye from a new perspective.

What was the hypothesis of the study?

Keratoconus eyes and healthy eyes show differences in aberrometry, not only in high-order terms (spherical, coma, trefoil), but also in extraordinary high-order aberrations.

What was learned from the study?

This prototype of aberrometer provides reliable ocular aberrometry values, and these are highly correlated with the corneal ones.

Keratoconus eyes are more likely to show micro-alteration (represented by the high-pass filtered map) in the ocular wavefront than healthy eyes.

or atopy [4], but it also correlates strongly with external factors such as eye rubbing, use of rigid contact lenses, or allergic eye disease [5]. Keratoconic corneas have an abnormal distribution and number of collagen fibril layers at the thinnest point, which increases tissue flexibility and alters the corneal mechanism [6]. Modern treatment techniques try to slow down the progression by reinforcing corneal tissue [7].

Findings from slit-lamp examination are indicative of severity and can reveal presence of stromal thinning, Vogt's striae, Fleischer rings, or corneal scarring. However, the introduction of keratoscopes in clinical practice has allowed early diagnosis and classification based on morphology or disease stage [8].

Elevation maps from corneal topography have been reported as sensitive screening methods, even in early-stage KC or forme fruste [9], furthermore new technology applied to those maps could improve the detection of the disease [10]. The point of maximal corneal elevation measured in diopters (Kmax) and the minimum value of the pachymetry map (PKmin) are two accurate and widely used indicators of KC progression [11–13], although more recent publications suggest that combinations of corneal parameters could be even more precise due to their high repeatability [13, 14]. Novel devices combining tomography and air-puff response that have been developed to measure the biomechanical properties of the cornea are promising but lag far behind other systems of KC detection and progression assessment on the basis of previous technology [15].

An alternative approach to KC classification involves measuring corneal aberrations with Zernike polynomials, in which primary coma or the root mean square (RMS) of coma-like aberrations, astigmatism, or higher-order aberrations (HOAs) are used as indicators [16]. These parameters showed good repeatability in mild-moderate KC, although the variability of this method must be taken into account when evaluating progression in severe cases [17]. However, KC screening methods based on optical aberration assessment are highly sensitive and specific [18].

INTRODUCTION

Keratoconus (KC) is a bilateral degenerative ocular disorder characterized by progressive stromal thinning and an abnormal, cone-like corneal shape that leads to visual impairment [1]. This multifactorial ectatic disease is traditionally described as a non-inflammatory condition [2], although recent studies suggest that inflammatory pathways may play an important role in its pathogenesis [3]. KC is commonly associated with Down's syndrome, Leber's congenital amaurosis, connective tissue disorders,

Ocular aberrations in patients with KC have been characterized by devices based on the Shack–Hartman (SH) sensors or laser ray tracing (LRT) [19, 20], the former more widely used for obtaining the ocular aberration phase directly. This technology allows phase-map sampling from 2600 measurement points with a pupil diameter of 9 mm (lateral resolution of 175 μm) for subsequent reconstruction and description with Zernike's polynomials up to sixth- or eight-order aberrations [21]. Some authors have pointed to sensor resolution as a limiting factor when calculating aberrations above the eighth order, and those coefficients might help to characterize or monitor ocular diseases [22–24]. According to the literature, SH devices exhibit high variability for HOAs, likely due to incorrect positioning of the spots in the image sensor, normally a charge-coupled device (CCD). These errors could be due to an overlapping of spot images or result from a high surface slope, which deviates the spot outside the sensor [25].

In this manuscript, we report on exploratory research in which patients with KC were examined by T-eyede, an aberrometer capable of obtaining the ocular phase at a lateral resolution of 8.55 μm . We expect that resolution power could result in more trustworthy assessment of the high-order aberration frequently used, not only to classify the stages of the KC, but also to describe their vision [26]. Furthermore, we want to explore the differences in terms of residual aberrations between patients with KC and healthy patients (after 10th order Zernike coefficient fitting), using a high-pass filter.

METHODS

This cross-sectional study was conducted in the Fundación Jiménez Díaz University Hospital. The local institutional review board approved the study protocol, which complies with the tenets of the Declaration of Helsinki. Informed consent was obtained from all subjects following an explanation of the nature and possible consequences of the study.

Apparatus

The T-eyede device (Wooptix S.L., San Cristóbal de La Laguna, Canary Islands, Spain) obtains phase data using the wavefront phase imaging (WFPI) sensor (Fig. 1a), which has a resolution of 8.6 μm for a pupil diameter of 9 mm [27]. This sensor captures two intensity images, shifted an equal distance to either side of the pupil plane over a conventional image detector as a CCD (Fig. 1b). Each pixel thus became a data point for phase determination, achieving the highest-resolution aberrometry measurements seen in the field of ophthalmology [28]. As a result, the wavefront phase can be described with extremely high orders of Zernike's polynomials, not yet analyzed to date (Fig. 1c). Based on the geometric propagation of light, this technique is capable of recovering the outgoing wavefront phase of the refractive sample, using the relationship between the intensity distribution map in both planes and the phase gradient on the Cartesian coordinates [29].

The device is a double-pass optical set-up that uses a super luminescent diode as its light source, with a wavelength of 785 nm and an exposure time of 30 ms in the pupil plane at a power of 0.78 mW [as required by the American National Standards Institute (ANSI)]. The light beam that emerges from the diode is collimated and directed toward the eye, passing through its components until it reaches the retina, which disperses the incoming light from back to front, providing a beam that carries complete ocular phase information. When this beam emerges from the eye, it is then redirected and resized by an optical system that corrects for defocus in the range of [−10.00 to +10.00 D]. After this, the beam is divided into two paths to obtain the intensity image of each plane at both sides of the pupil plane with the use of a camera (termed science camera) [27, 28].

To ensure correct alignment of the patient with the system, and correspondence between the pupil and sensor planes, the device is out-fitted with another camera that monitors the position of the patient, who is placed with their chin on the chinrest. The camera's reference allows the apparatus to be displaced in the three

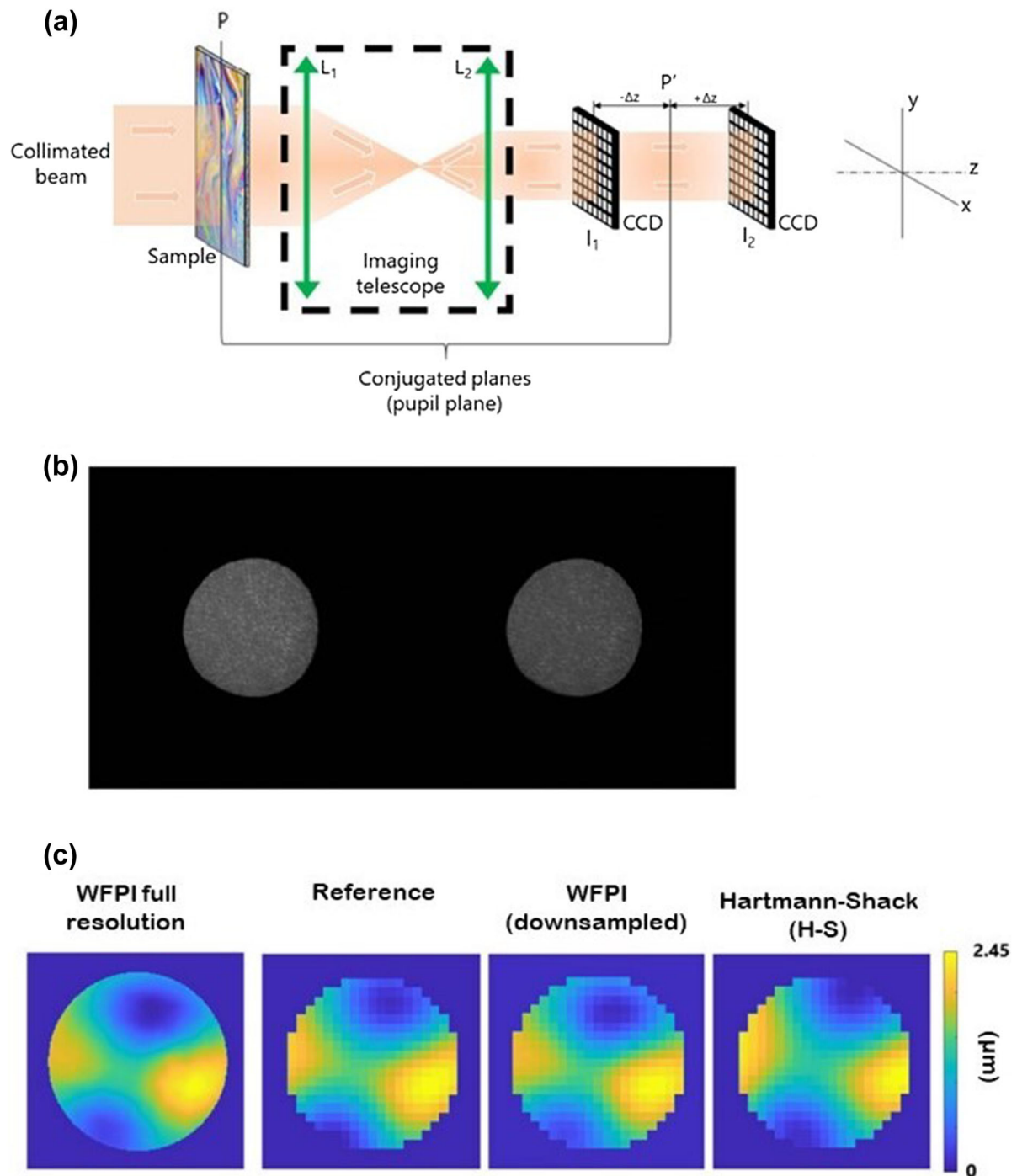


Fig. 1 **a** Wavefront phase imaging (WFPI) sensor technique principle scheme for transparent samples. **b** The pair of intensity images captured by the sensor. **c** The full resolution phase reconstructed from the two images obtained with WFPI, compared with the Hartmann–Shack

sensor resolution. Adapted from Bonaque-González et al. 2021 [27]. This article is distributed under the terms of the Creative Commons CC BY license, which permits unrestricted use, distribution, and reproduction

perpendicular directions until the pupil is properly centered and focused.

Corneal Aberrations

Corneal tomography was performed using the Pentacam HR camera system (Oculus Optikgeräte GmbH, Wetzlar, Germany), which obtains cross-sectional images with two rotating Scheimpflug cameras capturing up to 138 000 elevation points. Using these coordinates, a three-dimensional reconstruction of both corneal surfaces is converted into maps for clinical guidance [28–31]. Zernike coefficients for corneal elevation were obtained for a 6-mm diameter and exported to Zemax software using a dynamic data exchange toolbox.

To assess corneal aberration, we built an optical model in Zemax OpticStudio (Ansys Inc.), similar to other research [30]. The entrance aperture diameter was fixed at 3 mm for an infrared wavelength of 785 nm (the same used by the T-eyede device). Two corneal surfaces were inserted with Zernike elevation values from Pentacam with a refractive index of 1.443. The refractive index used for aqueous and vitreous was 1.3346. Anterior chamber depth was also imported from the Pentacam, and a third surface emulating the pupil was inserted with an automatic diameter. This process was automated for each subject using custom routines written in the Python language. The merit function used to optimize the position of the image plane was the default RMS wavefront for the centroid using a lenslet array of 64×64 . Finally, the first 45 terms of the Zernike coefficients were collected in standard notation. A sign correction for left eyes was performed in vertical axis symmetrical aberrations to avoid enantiomorphism bias (Fig. 2).

Variables

The topographical variables we collected were the most elevated point of the front surface in diopters (Kmax), the thinnest pachymetry value (PKmin), corneal astigmatism derived from simulated keratometry, and mean keratometry (Km). The keratoconus severity scale used was

based on the topographical keratoconus classification (TKC) of the Pentacam HR [31]. This scale spans stage 0 (healthy cornea) to stage IV (severe KC); additionally, a label of “possible” was used for borderline cases. Corneal aberration analysis included Zernike polynomial calculations up to the eighth order; we used the elevation Zernike polynomial (EZ) when describing anterior and posterior corneal surfaces for a 6-mm diameter and computed the wavefront Zernike polynomial for the entire cornea for a pupil with a diameter of 3 mm. Comparisons were made using the RMS for primary astigmatism ($Z 2 \pm 2$), primary coma ($Z 3 \pm 1$), coma-like aberrations ($Z 3 \pm 1$, $Z 5 \pm 1$, $Z 7 \pm 1$), or the coefficients of HOAs.

Ocular aberration analysis with T-eyede follows a two-step approach. First, a phase map represents the first 65 Zernike coefficients, except piston, tip/tilt, and defocus. Another phase map, named extremely high-order aberration map, determines Zernike polynomials up to the tenth order. Then, custom image-processing software routines are applied [27] and converted to a high-pass filter map (HPFM).

Ophthalmological examination included slit-lamp microscopy, recording signs of corneal ectasia such as Vogt’s striae or corneal scarring. Refraction variables such as best corrected visual acuity (BCVA) on the decimal scale and subjective refraction were also analyzed.

Patient Selection

This study was carried out in a volunteer cohort with no ocular diseases, as well as a group of patients with KC diagnosed by three experienced ophthalmologists. Diagnostic criteria for KC were based on abnormal values obtained for sensitive corneal topographical variables such as Kmax, PKmin, presence of irregular or asymmetric astigmatism, or analyzing the map of the best-fit toric ellipsoid with fixed eccentricity (BFTEFE) [32]. An additional diagnostic criterion for KC was the presence of signs in slit-lamp examination, including stromal thinning, Vogt’s striae, Fleischer ring, or corneal scarring. Furthermore, the TKC of Pentacam was studied and compared with physician criteria.

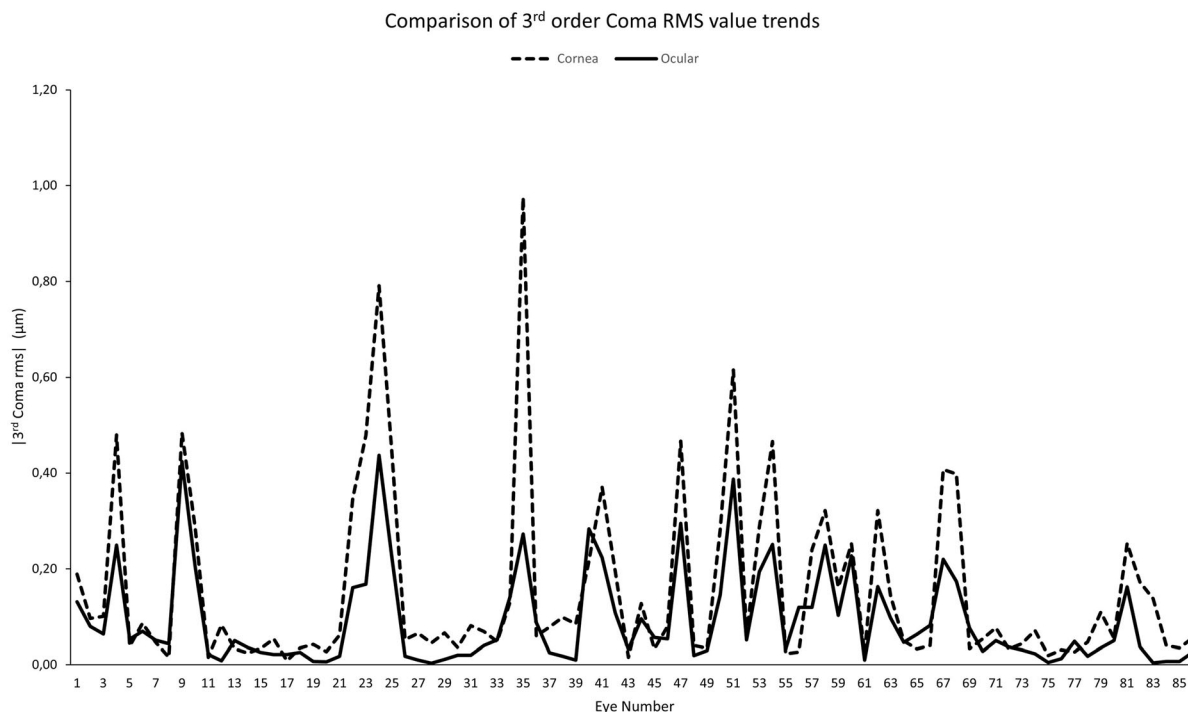


Fig. 2 Linear plot of RMS of primary coma for every patient, distinguishing between corneal and ocular aberration

The exclusion criteria were other ocular diseases, presenting with keratoconus, age under 18 years, current pregnancy or breastfeeding, or participation in another interventional study approximately 30 days prior to starting this study. Contact-lens wearers from the KC group were advised to suspend lens use at least one week before the clinical examination; no individuals in the control group wore contact lenses.

Statistical Analysis

Statistical analysis was performed using SPSS IBM version 28.0.1.1 (Chicago, IL, USA) software. Statistical significance was set at p values < 0.05 . The Shapiro–Wilk test was used to test for normal distribution of the samples, Mann–Whitney U test was used to compare features between the keratoconus and control group, and comparisons between corneal and ocular aberrations were performed by means of

the Wilcoxon test. Between-group comparisons were performed by chi-squared test.

RESULTS

This study comprised 43 eyes (25 patients, 15 females and 10 males) in the control group and 43 eyes (27 patients, 11 females and 16 males) in KC group. Healthy patients were 40.16 ± 9.84 (range 27–58) years old and keratoconus subjects were 38.42 ± 11.71 (range 18–66) years old.

Ophthalmological Examination

During slit-lamp examination, two right eyes from two different patients showed corneal scarring, and five eyes from three male patients presented signs of Vogt striae. Values for spherical equivalent and refractive cylinder were lower in the control group ($-0.5 [-3, 0]$ D and $-0.5 [-1, 0]$ DC) when compared with the KC group ($-2 [-3.25, -1]$ D and $-2[-3,$

– 1.25] DC, respectively); these refraction differences were statistically significant ($p < 0.001$). BCVA was high considering all patients, though a significant difference was found between groups ($p < 0.05$), as the control group had better results (1[1, 1.2] decimal units) than the KC group (0.9[0.7, 1] decimal units).

Corneal Tomography

Topographical variables such as Km, PKmin, Kmax, and corneal astigmatism presented higher values among patients diagnosed with KC than those in the control group. A more detailed analysis of descriptive data and the differences found is reported in Table 1.

Based on Pentacam keratoconus classification (TKC classification), 43 out of 86 eyes were classified as “healthy,” only one of which was in the KC group. Six were labeled as “possible:” five from the KC group and one in the control group. A total of 37 were classified as unhealthy corneas: 12 KC stage I, 21 KC stage II, 2 KC stage III, and 2 KC stage IV.

Considering the front corneal surface shape assessed by RMS of the Zernike polynomials of elevation data, the RMS of the primary coma for the control group was 0.546 [0.39, 0.871] μm , whereas the same variable in the KC group rose to 5.115 [2.723, 7.532] μm . A similar result was obtained when considering more coefficients of coma, as RMS coma-like was 0.558 [0.394,

0.882] μm for healthy corneas, while for the KC group it was 5.247 [2.75, 7.636] μm . When the rest of the higher-order coefficients were included, the results tended to be stable, as RMS HOAs for the normal corneas was 1.816 [1.641, 1.996] μm , while for the ectactic corneas it was 5.774 [3.73, 8.349] μm . A high level of statistical significance was reached for all the aforementioned variables between groups ($p < 0.001$).

The posterior corneal surface also presented significant shape differences between groups ($p < 0.001$), with patients from the control group showing lower RMS values than the KC group. For the first group, RMS primary coma was 1.065 [0.662, 1.409] μm , RMS coma-like was 1.15 [0.832, 1.474] μm , and RMS HOAs was 4.548 [4.176, 4.887] μm ; and for the KC group, these results were 10.45 [7.157, 16.49] μm , 10.686 [7.247, 16.654] μm , and 14.355 [11.09, 18.56] μm , respectively.

Optical Aberrations

Corneal wavefront aberrations obtained by custom ray tracing eye model presented higher values than ocular wavefront aberrations measured by T-eyede; these differences were statistically significant for the whole dataset. The median RMS of the primary astigmatic terms ($Z 2 \pm 2$) decreased by 0.145 μm , which indicates 51% crystalline lens cushioning. RMS of the primary coma ($Z 3 \pm 1$) was also mitigated, with

Table 1 Summary of values for corneal features of interest and comparison between control and study groups

Variable	Group	Median [Q1, Q3]	Mann–Whitney <i>U</i> test <i>p</i> value
Maximum keratometry (Kmax)	Control	43.9 [43, 45] D	< 0.001
	Keratoconus	51.7 [48.2, 54.4] D	
Minimum pachymetry (PKmin)	Control	556 [538, 576] μm	< 0.001
	Keratoconus	487 [451, 504] μm	
Mean keratometry (Km)	Control	43.16 [15, 42, 44] D	< 0.001
	Keratoconus	45.92 [44.91, 47.17] D	
Corneal astigmatism	Control	0.8 [0.35, 1] D	< 0.001
	Keratoconus	2.6 [2.05, 3.8] D	

a median change of $-0.017 \mu\text{m}$ (25%). For RMS of the coma-like aberrations (including coma terms of the fifth and seventh order), the difference is also 25% of the corneal aberration. The spherical corneal aberration (Z40) was $0.014 [0.007, 0.025] \mu\text{m}$, while the median measurement with T-eyede was $0.009 [0.003, 0.023] \mu\text{m}$. For HOAs, the median reduction in RMS was -0.034 (from $0.105 [0.072, 0.274]$ to $0.071 [0.043, 0.156]$) μm ; despite the small size of this change, it was significant statistically according to Wilcoxon signed-rank test ($p < 0.001$). Further statistical analysis, taking into consideration both groups, appears in Table 2.

Regarding the analysis of HPFM, we observed certain patterns. Thirty-five out of 86 maps (41%) evidenced a rough surface with proliferation of deep banding pattern or zones with low spatial frequencies out of focus, and 51 (59%) presented smooth and fine details in these maps (see Fig. 3 for an example).

Forty-one (95%) control patients exhibited a smooth HPFM and high-frequency patterns, 2 (ID_20 and ID_71) out of 43 (5%) showed presence of an irregular surface on HPFM; more information on these results appear in the supplementary material, and these findings are commented on at length in the discussion section below. In the KC group, 33 eyes (77%) showed banding patterns, while 10 out of 43 (23%) did not, comprising 8 which were cataloged as early-stage (possible or stage I) by Pentacam TKC and 2 as moderate (stage II).

The proportion of banding pattern presence on HPFM was statistically different between the control group and KC group as determined by chi-squared test (χ^2 (dof = 1, $N = 86$) = 43.36, $p < 0.001$), showing a large effect size (Phi value of 0.61). Exploring the dependency of irregular HPFM on KC classification, 17% of the cases labeled as “possible” presented this phenomenon, as did 75% of those labeled as stage I, 90% labeled stage II, and 100% of cases labeled as stage III and IV.

Regarding the relationship between KC classification and presence of a banding pattern on HPFM, this correlation was found in 17% of cases labeled as “possible.” The same occurred in 58% of the sample in KC stage I, 71% in stage II,

Table 2 Descriptive data of corneal and ocular optical aberration and comparison between the healthy and keratoconus (KC) groups, represented by median values [IQ1, IQ3]

	Control group		Wilcoxon signed-rank test		KC group		Wilcoxon signed-rank test	
	Cornea	Ocular			Cornea	Ocular		
RMS primary coma (μm)	0.044 [0.033, 0.068]	0.021 [0.011, 0.032]	$p < 0.001$		0.217 [0.071, 0.384]	0.141 [0.075, 0.224]	$p < 0.001$	
RMS coma-like (μm)	0.044 [0.033, 0.068]	0.021 [0.012, 0.032]	$p < 0.001$		0.217 [0.071, 0.385]	0.141 [0.075, 0.225]	$p < 0.001$	
RMS astigmatism (μm)	0.18 [0.132, 0.236]	0.082 [0.052, 0.14]	$p < 0.001$		0.49 [0.32, 0.725]	0.237 [0.146, 0.413]	$p < 0.001$	
RMS HOAs (μm)	0.072 [0.063, 0.095]	0.043 [0.031, 0.051]	$p < 0.001$		0.283 [0.174, 0.43]	0.159 [0.094, 0.272]	$p < 0.001$	

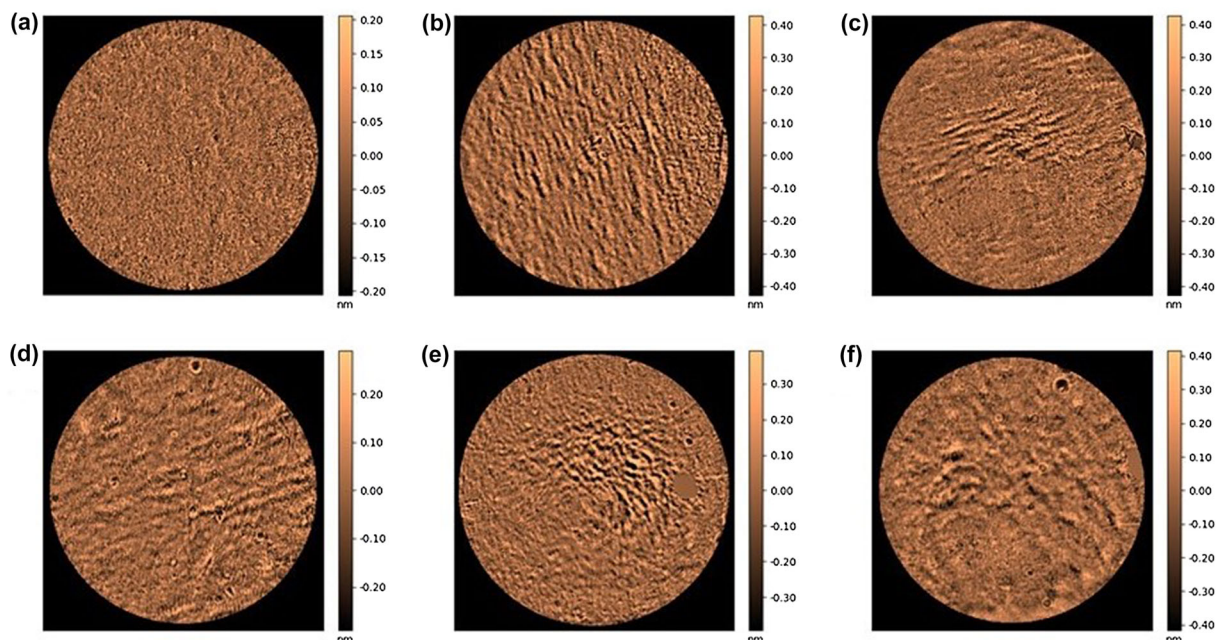


Fig. 3 High-pass filter map (HPFM) analysis patterns cataloged in millimeters. **a** Represents a smooth HPFM surface of a healthy patient (ID: 15). **b** Shows a banding pattern from an early stage of keratoconus (KC) (ID: 5). **c** and **d** Two moderate cases of KC, which showed

different shapes of banding patterns, ID: 9 and 22, respectively. **e** and **f** Two different curve banding or irregular patterns from two patients with advanced and severe KC, ID: 41 and 24, respectively

and 100% in both stages III and IV. The result of a chi-squared test of independence for KC classification and an irregular pattern on the HPFM was χ^2 (dof = 5, $N = 86$) = 57.83, $p < 0.001$.

DISCUSSION

The etiology of KC remains unclear, despite numerous efforts to find a correlation with systemic diseases or environmental factors [33, 34]. There is a currently unmet need for deeper understanding of the disease mechanisms, and for methods that contribute to accurate characterization of corneal properties and early detection [35, 36]. In this study, we applied an innovative aberrometer with a lateral resolution of 8.55 μm to the clinical study of patients with KC disease. The results reveal not only high-precision assessment of optical aberrations and fuller understanding of patient vision, but also offer a description of novel

image-processing techniques that could aid in KC diagnosis.

Diagnostic methods for KC are constantly being refined with the implementation of new technologies and in light of comprehensive research on the topic [9, 15, 37, 38]. The diagnostic criteria used in this study followed widely used consensus methods [39] and included measurement of posterior corneal elevation, which could lead to better screening results, even in forme fruste KC [32]. The heterogeneous presentation of KC disease is a handicap for aberrometry, and taking measurements in more advanced stages of the disease can be challenging. In this study, the maximum Km value for the KC group was 51.57 D, which is similar to previous studies [40, 41]. However, Km is not the most suitable index to classify KC stage, as vertical coma ($Z_{3,-1}$) is the most characteristic aberration of this disease and a good predictor of severity. In this study, the median RMS for elevation primary coma was 5.247 μm with a range from 1.53 to 17.85 μm , a median

value classified as advanced KC (Stage IV) by other authors [18].

Regarding the healthy group, mean ocular aberrations provided by T-eyede resembled those described by Applegate et al. [42], and the maximum value for each measurement was within the expected upper-limit value for the selected pupil and age range [43]. Nevertheless, we did not find normal aberration values for 3-mm pupils from patients with KC. The aberration measurements suggest that internal structures tend to absorb a substantial part of corneal aberrations, as described by Atchison et al. in 2016 [44]. In this study, the crystalline lens reduced the mean ocular HOAs (32%), RMS astigmatism (51%), and RMS for primary coma (25%), similar to other studies [41, 45], though a divergent trend was found between groups. Gordon-Shaag et al. found lower rates of compensation, due to internal aberration for RMS of primary coma and astigmatism, than in our study, possibly because aberration absorption by crystalline lenses depends not only on the direction of the coefficient, but also seems to be related to individual patient refraction [46].

According to the literature, nearly half of KC cases present with signs such as Vogt striae on slit-lamp examination [47], which are related to the banding pattern observed using confocal microscopy in 73% of patients with KC [48]. This sign resembles the irregular presence of bands in the HPFM of this study; however, the two devices are based on different principles and should be carefully studied. Mocam et al. hypothesize that this light–dark pattern could be produced by a change in the arrangement of some corneal lamellae resulting from the altered corneal shape, and these authors performed a thorough analysis of each corneal layer and its abnormalities. The T-eyede device captures the wavefront phase emerging from the eye in a more general manner, taking information from all the structures of the eye and delimited by the patient's pupil. Nevertheless, the results of the current study displayed in HPFM suggest that the abnormal structure of the KC corneal tissue interacts with light, and the phase of the ocular wavefront is affected. To the best of our knowledge, this is the first time this phenomenon has been detected at this

level detail, and it is due to the high-resolution power of this aberrometer.

Two eyes (20th and 71st) within the control group showed a banding pattern in HPFM, and more information about these eyes, such as Pentacam topography maps and PK progression analysis appears in the supplementary material. The eye with ID: 20 showed an oblique astigmatism of 1.5 D, normal corneal values for Km (44.61D) and PKmin (572 μm), and the front corneal surface RMS for the primary coma was 0.375 μm , which is close to the cut-off value (0.377 μm) for diagnosis of KC suggested by Ortiz-Toquero et al. [18]. In addition, this eye showed an abnormal value for vertical coma (Z3-1) on the anterior corneal surface of +1.437 μm , which is far from the control group mean of Z3-1 (−0.129 μm). In contrast, the eye with ID: 71 showed a normal anterior corneal surface (Km = 41.28D, Kmax = 42 D, Pkmin = 555 μm , and Z3-1 = 0.226 μm), although the posterior vertical coma was −1.74 μm and the elevation map (BFTEFE) revealed a +8 μm at the minimum pachymetry point.

Ten eyes of the KC group presented no irregular patterns on HPFM analysis. Corneal tomography showed that some of these had a cone apex far from the pupil center. One hypothesis could be that the damaged tissue, which produced the light distortion, is outside of the analysis diameter of the T-eyede device. Extending this diameter could be a possible solution, although the larger the area analyzed, the greater the likelihood of error in the location of spots on the aberrometer. Another solution could be to decenter the measurement with respect to the line of sight, although doing so would induce aberration coefficients that do not represent the normal vision of the patient.

However, the findings of this study must be seen in light of some limitations. Firstly, this HPFM map deserves further study given that it is taken from the whole path of the light, including internal ocular aberrations and possible crystalline lens issues, such as vacuoles in the crystalline lens or any type of cataract. On the other hand, the participants in this study were young and crystalline lens opacifications are rare for this age. Furthermore, a more

advanced version of the T-eyede aberrometry system is under development. This new device will be able to change the distance between image planes, making it more sensitive to smaller structures, and enhancing its ability to distinguish among ocular components. Once completed, this device will allow us to study individual structures of the human eye and characterize its optical properties separately.

Another restriction was to choose a small pupil radius for the analysis of the optical aberrations. To measure highly aberrant KC eyes, we needed to select a relatively low diameter of analysis (3 mm), while most previous studies are designed to assess a 6-mm pupil. Nevertheless, some studies have used this same pupil diameter for healthy patients [42, 43], and ours could be the first study to describe high-precision ocular aberration in patients with KC for this pupil size.

Another limitation concerns interpretation of presence or absence of a banding pattern in the HPFM. For this reason, every map was independently reviewed by three researchers (G.V.R., C.B.P., N.A.A.), and all HPFM results are available from the corresponding author on reasonable request. Our next step will be to perform a numerical analysis of the HPFM and vary the frequency filter to explore a new KC classification, and thereby increase the sensitivity. Finally, we find another limitation in the lack of previous research studies using this technology on clinical practice. It is important to highlight that the device used in this study is a prototype and it is not in the market. Therefore, the findings of this investigation cannot be applied to the daily clinical practice at this moment. We are aware that this technology is in an early stage of development for this field and more studies are needed.

CONCLUSION

This study demonstrates that the T-eyede device is able to measure KC eyes across a wide range of disease stages. The ocular aberration measures provided by the system are reliable and precise, and correlate well with corneal aberrations. T-eyede has an extraordinary resolution that is

capable of capturing small details of the human eye wavefront, and in this study, we found a correlation between the HPFM and the KC diagnosis.

ACKNOWLEDGEMENTS

We want to thank all the optometrists and physicians from the Ophthalmology Department of Fundación Jiménez Díaz University Hospital for their efforts in this project. We also are grateful to Dr. Miguel Faria for validation of the Zemax eye model and the Zernike coefficient assessment.

Funding. Funding for editorial assistance and the journal's Rapid Services Fee were provided by Wootix, S.L.

Medical Writing/Editorial Assistance. The authors wish to acknowledge Oliver Shaw, PhD (freelance medical editor) for editorial assistance.

Author Contributions. Gonzalo Velarde-Rodríguez: Writing - Original Draft, Conceptualization, Investigation, Formal analysis, Visualization. Carolina Belda-Para: Writing - Original Draft, Software, Validation, Investigation, Visualization. Miriam Velasco-Ocaña: Software, Validation, Writing - Review & Editing. Juan M. Trujillo-Sevilla: Software, Validation. Javier Rodríguez-Martin: Writing - Review & Editing. Ignacio Jiménez-Alfaro: Supervision, Resources. José M. Rodríguez-Ramos: Review & Editing, Supervision, Resources, Funding acquisition. Nicolás Alejandro-Alba: Conceptualization, Methodology, Project administration, Review & Editing.

Disclosures. Gonzalo Velarde-Rodríguez, Nicolás Alejandro-Alba, Ignacio Jiménez-Alfaro and Javier Rodríguez-Martin have nothing to disclose. Carolina Belda-Para, Miriam Velasco-Ocaña, Juan M. Trujillo-Sevilla are employees of Wootix S.L. Jose M. Rodríguez-Ramos is Chief Executive officer at Wootix S.L.

Compliance with Ethics Guidelines. The study protocol complies with the tenets of the Declaration of Helsinki and Ethics Committee approval was obtained from Comité de Ética de la Investigación Fundación Jiménez Díaz in April 2021 (reference number: PIC032_21). Informed consent was obtained from all subjects following an explanation of the nature and possible consequences of the study.

Data Availability. The data that support the findings of this study are available from the corresponding author (GVR) upon reasonable request.

Open Access. This article is licensed under a Creative Commons Attribution-NonCommercial 4.0 International License, which permits any non-commercial use, sharing, adaptation, distribution and reproduction in any medium or format, as long as you give appropriate credit to the original author(s) and the source, provide a link to the Creative Commons licence, and indicate if changes were made. The images or other third party material in this article are included in the article's Creative Commons licence, unless indicated otherwise in a credit line to the material. If material is not included in the article's Creative Commons licence and your intended use is not permitted by statutory regulation or exceeds the permitted use, you will need to obtain permission directly from the copyright holder. To view a copy of this licence, visit <http://creativecommons.org/licenses/by-nc/4.0/>.

REFERENCES

- Krachmer JH, Feder RS, Belin MW. Keratoconus and related noninflammatory corneal thinning disorders. *Surv Ophthalmol*. 1984;28(4):293–322.
- Nordan LT. Keratoconus: diagnosis and treatment. *Int Ophthalmol Clin*. 1997;37(1):51–63.
- Wisse RPL, Kuiper JJW, Gans R, Imhof S, Radstake TRDJ, van der Lelij A. Cytokine expression in keratoconus and its corneal microenvironment: a systematic review. *Ocular Surface*. 2015;13(4):272–83.
- Rabinowitz YS. Keratoconus. *Surv Ophthalmol*. 1998;42(4):297–319.
- Sahebjada S, Al-Mahrouqi HH, Moshegov S, et al. Eye rubbing in the aetiology of keratoconus: a systematic review and meta-analysis. *Graefes Arch Clin Exp Ophthalmol*. 2021;259(8):2057–67.
- Davidson AE, Hayes S, Hardcastle AJ, Tuft SJ. The pathogenesis of keratoconus. *Eye (Lond)*. 2014;28(2):189–95.
- Borroni D, Bonzano C, Hristova R, Rachwani-Anil R, Sánchez-González JM, de Lossada CR. Epithelial flap corneal cross-linking. *J Refract Surg*. 2021;37(11):741–5.
- Krumeich JH, Daniel J, Knalle A. Live-epikeratophakia for keratoconus. *J Cataract Refract Surg*. 1998;24(4):456–63.
- Belin MW, Duncan JK. Keratoconus: the ABCD grading system. *Klin Monbl Augenheilkd*. 2016;233(6):701–7.
- Chen X, Zhao J, Iselin KC, et al. Keratoconus detection of changes using deep learning of colour-coded maps. *BMJ Open Ophthalmol*. 2021;6(1):e000824.
- Wajnsztajn D, Shmueli O, Zur K, Frucht-Pery J, Solomon A. Predicting factors for the efficacy of cross-linking for keratoconus. *PLoS ONE*. 2022;17(2):e0263528.
- Hashemi H, Panahi P, Asgari S, Emamian MH, Mehravaran S, Fotouhi A. Best indicators for detecting keratoconus progression in children: a report from the shahroud schoolchildren eye cohort study. *Cornea*. 2022;41(4):450–5.
- Shajari M, Steinwender G, Herrmann K, et al. Evaluation of keratoconus progression. *Br J Ophthalmol*. 2019;103(4):551–7.
- Yousefi A, Hashemi H, Khanlari M, Amanzadeh K, Aghamirsalim M, Asgari S. Keratometric indices for detecting the type of keratoconus: a combined discriminant analysis. *Clin Exp Optom*. 2020;103(4):463–8.
- Zhang H, Tian L, Guo L, et al. Comprehensive evaluation of corneas from normal, forme fruste keratoconus and clinical keratoconus patients using morphological and biomechanical properties. *Int Ophthalmol*. 2021;41(4):1247–59.
- Alió JL, Shabayek MH. Corneal higher order aberrations: a method to grade keratoconus. *J Refract Surg*. 2006;22(6):539–45.

17. Tunç U, Akbaş YB, Yıldırım Y, Kepez Yıldız B, Kırgız A, Demirok A. Repeatability and reliability of measurements obtained by the combined Scheimpflug and Placido-disk tomography in different stages of keratoconus. *Eye (Lond)*. 2021;35(8):2213–20.
18. Ortiz-Toquero S, Fernandez I, Martin R. Classification of keratoconus based on anterior corneal high-order aberrations: a cross-validation study. *Optom Vis Sci*. 2020;97(3):169–77.
19. Maeda N, Fujikado T, Kuroda T, et al. Wavefront aberrations measured with hartmann-shack sensor in patients with keratoconus. *Ophthalmology*. 2002;109:1996–2003.
20. Barbero S, Marcos S, Merayo-Llodes J, Moreno-Barriuso E. Validation of the estimation of corneal aberrations from videokeratography in keratoconus. *J Refract Surg*. 2002;18(3):263–70.
21. Plaza-Puche AB, Salerno LC, Versaci F, Romero D, Alio JL. Clinical evaluation of the repeatability of ocular aberrometry obtained with a new pyramid wavefront sensor. *Eur J Ophthalmol*. 2019;29(6):585–92.
22. López-Miguel A, Maldonado MJ, Belzunce A, Barrio-Barrio J, Coco-Martín MB, Nieto JC. Precision of a commercial hartmann-shack aberrometer: limits of total wavefront laser vision correction. *Am J Ophthalmol*. 2012;154(5):799–807.e5.
23. Piñero DP, Alió JL, Alesón A, Escaf M, Miranda M. Pentacam posterior and anterior corneal aberrations in normal and keratoconic eyes. *Clin Exp Optom*. 2009;92(3):297–303.
24. Prieto PM, Vargas-Martin F, Goelz S, Artal P. Analysis of the performance of the Hartmann-Shack sensor in the human eye. *J Opt Soc Am A Opt Image Sci Vis*. 2000;17(8):1388.
25. Jinabhai A, Radhakrishnan H, O'Donnell C. Repeatability of ocular aberration measurements in patients with keratoconus. *Ophthalmic Physiol Opt*. 2011;31(6):588–94.
26. Rozema JJ, Hastings GD, Jiménez-García M, Koppen C, Applegate RA. Assessing the visual image quality provided by refractive corrections during keratoconus progression. *Ophthalmic Physiol Opt*. 2022;42(2):358–66.
27. Bonaque-González S, Trujillo-Sevilla JM, Velasco-Ocaña M, et al. The optics of the human eye at 8.6 μm resolution. *Sci Rep*. 2021;11(1):23334.
28. Bonaque-González S, Trujillo-Sevilla JM, Casanova-Gonzalez O, et al. New high-resolution wave front sensing ophthalmic technique for the characterization of ocular optics. Published online February 19, 2020:67.
29. Trujillo-Sevilla JM, Casanova Gonzalez O, Bonaque-González S, Gaudestad J, Rodríguez Ramos JM. High-resolution wave front phase sensor for silicon wafer metrology. Published online March 4, 2019: 18.
30. Pérez-Merino P, Marcos S. Effect of intraocular lens decentration on image quality tested in a custom model eye. *J Cataract Refract Surg*. 2018;44(7):889–96.
31. Spira C, Grigoryan A, Szentmáry N, Seitz B, Langenbacher A, Eppig T. Vergleich der Spezifität und Sensitivität verschiedener gerätegestützter Keratokonusindizes und -klassifikatoren. *Ophthalmologie*. 2015;112(4):353–8.
32. Garcerant D, Jiménez-Alfaro I, Alejandro N, Remon L. Diagnostic sensitivity of different reference bodies when using scheimpflug tomography in a myopic population with keratoconus. *J Ophthalmol*. 2019;2019:1–7.
33. Hashemi H, Heydarian S, Hooshmand E, et al. The prevalence and risk factors for keratoconus: a systematic review and meta-analysis. *Cornea*. 2020;39(2):263.
34. Seth I, Bulloch G, Vine M, et al. The association between keratoconus and allergic eye diseases: a systematic review and meta-analysis. *Clin Exp Ophthalmol*. 2022;50(3):280–93.
35. Zhang H, Zhang X, Hua L, et al. An exploratory analysis of forme fruste keratoconus sensitivity diagnostic parameters. *Int Ophthalmol*. 2022;42(8):2473–81.
36. Kwok S, Pan X, Liu W, Hendershot A, Liu J. High-frequency ultrasound detects biomechanical weakening in keratoconus with lower stiffness at higher grade. *PLoS ONE*. 2022;17(7): e0271749.
37. Vellara HR, Patel DV. Biomechanical properties of the keratoconic cornea: a review. *Clin Exp Optom*. 2015;98(1):31–8.
38. Belin MW, Jang HS, Borgstrom M. Keratoconus: diagnosis and staging. *Cornea*. 2022;41(1):1–11.
39. Gomes JAP, Tan D, Rapuano CJ, et al. Global consensus on keratoconus and ectatic diseases. *Cornea*. 2015;34(4):359–69.
40. Naderan M, Jahanrad A, Farjadnia M. Ocular, corneal, and internal aberrations in eyes with keratoconus, forme fruste keratoconus, and healthy eyes. *Int Ophthalmol*. 2018;38(4):1565–73.

41. Gordon-Shaag A, Millodot M, Ifrah R, Shneor E. Aberrations and topography in normal, keratoconus-suspect, and keratoconic eyes. *Optom Vis Sci.* 2012;89(4):411–8.
42. Applegate RA, Donnelly WJ III, Marsack JD, Koenig DE, Pesudovs K. Three-dimensional relationship between high-order root-mean-square wavefront error, pupil diameter, and aging. *J Opt Soc Am A Opt Image Sci Vis.* 2007;24(3):578.
43. Bruce AS, Catania LJ. Clinical applications of wavefront refraction. *Optom Vis Sci.* 2014;91(10):1278–86.
44. Atchison DA, Suheimat M, Mathur A, Lister LJ, Rozema J. Anterior corneal, posterior corneal, and lenticular contributions to ocular aberrations. *Invest Ophthalmol Vis Sci.* 2016;57(13):5263–70.
45. Kelly JE, Mihashi T, Howland HC. Compensation of corneal horizontal/vertical astigmatism, lateral coma, and spherical aberration by internal optics of the eye. *J Vis.* 2004;4(4):262–71.
46. Taberero J, Benito A, Alcón E, Artal P. Mechanism of compensation of aberrations in the human eye. *J Opt Soc Am A Opt Image Sci Vis.* 2007;24(10):3274.
47. Szczotka LB, Barr JT, Zadnik K. A summary of the findings from the Collaborative Longitudinal Evaluation of Keratoconus (CLEK) Study. CLEK Study Group. *Optometry.* 2001;72(9):574–84.
48. Mocan MC, Yilmaz PT, Irkeç M, Orhan M. The significance of Vogt's striae in keratoconus as evaluated by in vivo confocal microscopy. *Clin Exp Ophthalmol.* 2008;36(4):329–34.